



A photocured bio-based shape memory thermoplastics for reversible wet adhesion



Yuchao Wu ^{a,1}, Changhua Su ^{b,1}, Shaoyun Wang ^a, Bujingda Zheng ^a, Alireza Mahjoubnia ^a, Kianoosh Sattari ^a, Hanwen Zhang ^c, James Meister ^d, Guoliang Huang ^a, Jian Lin ^{a,*}

^a Department of Mechanical and Aerospace Engineering, University of Missouri, Columbia, MO 65211, USA

^b Food Science Program, Division of Food, Nutrition & Exercise Sciences, University of Missouri, Columbia, MO 65211, USA

^c Department of Chemical and Biomedical Engineering, University of Missouri, Columbia, MO 65211, USA

^d Department of Civil and Environmental Engineering, University of Missouri, Columbia, MO 65211, USA

ARTICLE INFO

Keywords:

Biopolymer
Shape memory
Shape locking
Wet adhesion

ABSTRACT

Development of reversible wet or underwater adhesives remains a grand challenge, because weakened intermolecular interactions by water molecules or/and low effective contact area cause poor interface to the wet surfaces, which significantly decreases adhesive strength. Herein, a new photocured, bio-based shape memory polymer (SMP) that shows both chemical and structural wet adhesion to various types of surfaces is developed. The SMP is polymerized from three monomers to form linear polymer chains dangled with hydrophobic side chains. The hydrogen acceptor and donor groups in the chains form hydrogen bonding with the surfaces, which is protected by the hydrophobic chains in the interface. The SMP shows tunable phase transition temperature (T_g) of 17–38 °C. In a rubbery state above T_g , the adhesive forms conformable contact with the targeted surfaces. Below T_g , a transition to a glassy state locks the conformed shapes to largely increase the effective contact area. As a result, the adhesive exhibits long-term underwater adhesion of >15 days with the best adhesion strength of ~0.9 MPa. Its applications in leak repair, underwater on-skin sensors were demonstrated. This new, general strategy would pave avenues to designing bio-based, long-lasting, and reversible adhesives from renewable feedstocks for widespread applications.

1. Introduction

Adhesives are widely used in our daily life [1,2]. They generally form permanent or reversible bonding with targeted surfaces, corresponding to glue- and tape-type adhesives, respectively [3,4]. The former is usually in a liquid state made of prepolymers [5] or monomers [6]. The adhesion to the surfaces is formed by a transformation from liquid to solid. This type of adhesion is usually irreversible and cannot be reused. On the contrary, the latter is usually in a solid state made of solid polymers [7] or hydrogels [8], whose adhesion is directly formed by reversible interactions of the substances with the surfaces. The interactions include van der Waals force, electrostatic force, and hydrogen bonding, while they can be significantly reduced by the hydration layer in a wet environment, resulting in debonding [9,10]. For instance, adhesion strength of a gecko foot pad to the surfaces is significantly weakened when it is wet [11]. Additionally, water is easily trapped at

interfaces of the substrates and adhesives, especially when the surfaces are rough. This not only reduces the effective contact area, but also introduces crack defects, thus largely decreasing the adhesive strength [4]. As a result, the weakened adhesion greatly limits the applications of the adhesives in leakage repair, biosensors for underwater usage, organ repair, and others [12,13].

Recently, researchers have successfully constructed special non-covalent interactions that are not weakened by the hydration layer, such as hydrophobicity interactions [14], host-guest interactions [7], and cation-π interactions [3] to ensure strong underwater bonding. Meanwhile, it is worth noting that most adhesives are synthesized from the petroleum sources [15], development of renewable bio-based underwater adhesives would afford an alternative green and sustainable pathway, which has been largely underexplored. Inspired by Liu's work [16], he proposed a strategy to protect hydrogen bonds by effective entanglement with a hydrophobic layer. It is reasonable to hypothesize

* Corresponding author.

E-mail address: linjian@missouri.edu (J. Lin).

¹ Equally contributed to the work.

that vegetable oils could offer a similar pathway to protect the hydrogen bonds as most of them consist of many long fatty acid hydrophobic chains.

On the other hand, besides the ways of enhancing chemical interactions, some physical interactions may be a promising method for creating the reversible wet adhesion, such as surface free energy, capillary force and biologically inspired structures [17–19]. Inspired by this, physical interaction may be designed to improve the contact area and prevents defect formation in the interfaces of the substrates and adhesives for creating strong wet adhesion. Shape memory polymers (SMPs), a class of stimulus responsive polymers [20], have shown promises in achieving this target [21]. They interconvert between the glassy and rubbery states with a dramatic change in modulus. They can be easily deformed above phase transition temperature (T_g) and memorize the deformed shape after cooled below T_g . For an adhesion application, they can conformably contact the topography of the targeted surfaces in the rubbery state (low modulus, easy to be deformed). This temporary shape can be memorized in the glassy state (high modulus, hard to be deformed) below T_g , thus forming an effect of mechanical interlocking in the interfaces. This structurally enhanced adhesion has been named a strong rubbery-to-glass (R2G) adhesion [21].

Herein, we report a design strategy of manipulating both chemical and structure interactions in a bio-based SMP for strong wet adhesion, e.g., a new photocured, bio-based SMP that shows both chemical and topography wet adhesion with various types of surfaces is developed. The adhesion can be reversible and repeatable. The SMP with tunable T_g was synthesized by radical photopolymerization of three monomers of 2-hydroxy-3-phenoxypropyl acrylate (HA), *N*-vinylpyrrolidone (NVP), and dodecyl acrylate (DA). These monomers were polymerized to a linear polymer chain, forming a thermoplastic. In the polymer chain, HA contains β -hydroxyl groups while NVP has oxocarbon anion groups. So, they can serve as hydrogen bond acceptors and donors, respectively, which contribute to the tough adhesion performance of the SMP. DA is derived from coconut oil. It contains a long fatty acid carbon chain, which is hydrophobic, thus can protect the hydrogen bonding (H-

bonding) in the SMP network from being weakened by the hydration layer of the wet surfaces. In addition, the SMP with tunable T_g of 17–38 °C offers a R2G adhesion capability to increase the adhesion strength by ~250 % compared to those without the R2G adhesion. Finally, the SMP is photocured, and the reversible, long-lasting adhesion performance was demonstrated in bonding different types of substrates, repairing a leak, and serving as an adhesive substrate for underwater on-skin bioelectronics, indicating a great promise of this material for widespread applications.

2. Results and discussion

2.1. Synthesis of the SMP adhesive

The proposed SMP was synthesized by an ink mixed with a soft monomer, DA with T_g of ~0 °C, and two hard monomers, HA with T_g of ~25 °C and NVP with T_g of ~100 °C. Upon UV irradiation, photo-initiator diphenyl(2,4,6-trimethylbenzoyl)phosphine oxide (TPO) will trigger the radical polymerization via the C = C bonds of these three monomers, forming linear thermoplastic polymer chains (Fig. 1a and Fig. S1). These chains contain abundant β -hydroxyl groups attributed from HA and the oxocarbon anion groups from NVP. These groups form hydrogen bonds among these polymer chains to toughen the polymer [22], meanwhile accelerating the polymerization rate owing to enhanced interactions of these two monomers in the liquid precursor [23]. In addition, these abundant β -hydroxyl groups can form H-bonds with polar or highly electronegative surfaces for adhesion. If these H-bonds are not protected, they tend to be weakened by the hydration layer in the wet interfaces. To mitigate this potential issue, DA, a monomer derived from the coconut oil, was deployed as part of the precursor. The hydrophobic fatty acid chains in DA are hypothesized to prevent water from direct contact with the H-bonds, thus can effectively protect the H-bonds from being weakened by the hydration layer (Fig. 1b). The photo-curability of the ink makes the synthesized SMP be patterned to different structures (Fig. 1c). Additionally, T_g of the thermoplastic polymer can be tuned to a range of 17–38 °C, which is much

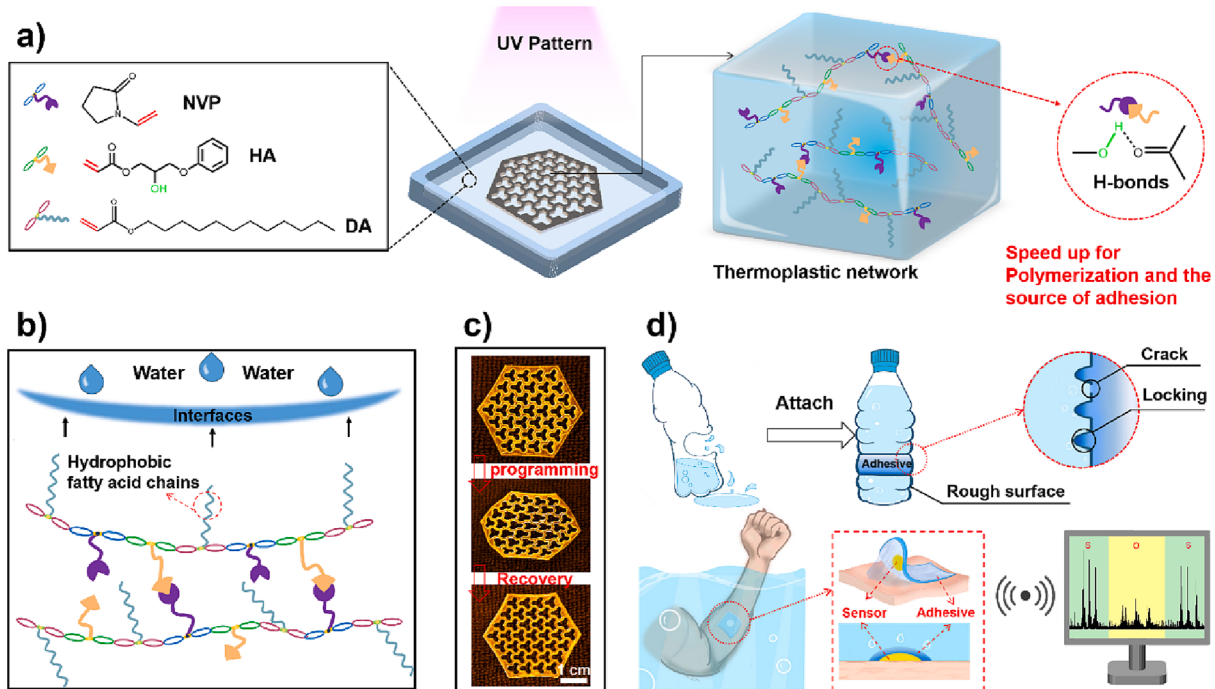


Fig. 1. Overview of the work. (a) Scheme showing photocuring of a SMP adhesive and its H-bond formation. (b) Scheme showing mechanism of using hydrophobic interactions for protecting H-bonds. (c) Photographs showing a shape memory cycle of a UV patterned SMP lattice. (d) Applications of the SMP adhesives in leakage repair and underwater sensors.

lower than those of thermosets [24], thus making the shape programming easier and faster. As shown in Fig. 1c and Video S1, the high-precision lattice structure was fabricated utilizing UV lithography. The lattice structure was programmed above its phase transition temperature and rapidly cooled, enabling it to memorize the programmed shape. Upon heating above the phase transition temperature, the lattice structure rapidly recovered to its original state. This combined strategy of using both chemical and structure interactions with the targeted wet surfaces for developing renewable SMP adhesives could lead to widespread applications. As demos, we applied it to repair a leaked bottle hole and used it as a substrate for underwater on-skin bioelectronics (Fig. 1d).

2.2. Mechanical and shape memory properties of the SMP adhesive

The adhesive is a thermoplastic polymer, and the mechanical properties and T_g can be tuned simply by weight ratios of the soft and hard monomers. To study the respective effects of the three monomers, we used a weight ratio of 2:1:1 for DA, HA, and NVP as a reference. To vary the mechanical properties and T_g of the SMPs, the ratios of the two monomers were fixed and the third one was tuned. For instance, the samples named DA-2.0, DA-2.4, DA-2.8, DA-3.2 refer to the ones polymerized with DA, HA, and NVP weight ratios of 2:1:1, 2.4:1:1, 2.8:1:1, and 3.2:1:1, respectively. See Methods for details. It is found that as the weight ratio was tuned, the viscosity of the ink varies in a range of 0.007–0.041 Pa·s (Fig. S2). The low viscosity of <1.3 Pa·s would facilitate the photopolymerization [25]. Interestingly, the viscosity increases with increase of the weight ratios of the HA monomer (Fig. S2b). This could be caused by the hydroxyl groups existing in HA. As the HA ratio increases, the H-bonding interactions increase [26]. It is found that mechanical properties of the SMPs depend on the weight ratios of the

soft and hard monomers. The stress-strain curves of Fig. 2a show a rubber-like behavior due to the flexible chains and lower T_g . The other SMPs show a clear plastic-to-rubber transition behavior (Fig. 2b–c). The stress-strain curves show a plastic-like behavior in the beginning. After the yield, the plastic-like behavior is transitioned to a rubber-like one, showing a rapidly increased stress, and is finally followed by fracture, thus resulting in a high ductility [27]. DA's chain is long and acts as a soft segment in the polymer network, making fractural strain of the synthesized material increase from 451 % to 614 % when the DA's weight ratio to HA and NVP increases from 2.0 to 3.2 (Fig. 2d). HA has rich hydroxyl groups that make the synthesized polymer chains form H-bonds, thereby increasing the tensile strength of the SMPs from 1.14 to 1.96 MPa when the weight ratios of HA increases from 1.0 to 2.2 (Fig. 2e), while maintaining a fractural strain of 369 % (Fig. 2d). Due to its rigid molecule structure, NVP acts as a hard segment in the polymer network. As its weight ratio increases from 1 to 2.2, the tensile strength of the materials is significantly improved from 1.14 to 7.47 MPa (Fig. 2e). The Young's module is increased from 0.49 to 14.61 MPa (Fig. 2f).

To study the recovery performance, cyclic tensile testing was performed on the DA-3.2 and NVP-2.2 samples (Fig. 2g–h). A hysteresis loop is seen in the cyclic curves, indicating great energy dissipation capability, which benefits energy absorption from external loading. The results also show that the adhesives have significant residual strain accompanied by a decrease in strength after a continuous circulation at a strain of ~80 % of the fractural strain. As shown in Fig. 2g, DA-3.2 shows more recoverable elastic deformation than NVP-2.2 does properly because of the flexibility of the long chains in DA. NVP-2.2 showing a larger residual strain. Nevertheless, the residual strains of both samples can be almost recovered after being heated up to ~70 °C. It could be because the flexibility of the thermoplastic network can easily relax the

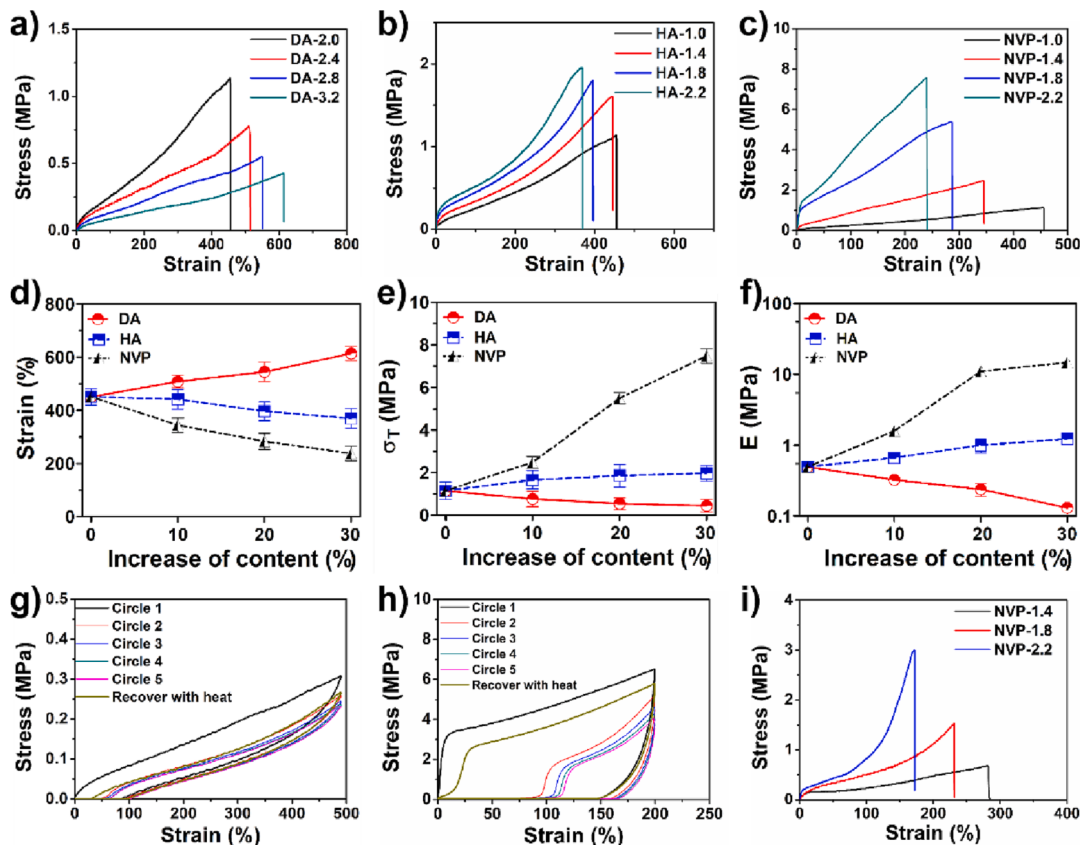


Fig. 2. Mechanical properties of the SMP adhesives. Stress-strain curves of the SMPs with different (a) DA; (b) HA; and (c) NVP ratios. Effect of monomer weight ratios on (d) strain; (e) tensile strength (σ_T); and (f) Young's modulus (E) of the SMPs. Cyclic tensile curves of (g) DA-3.2 and (h) NVP-2.2 samples. (i) Stress-strain curves of NVP-1.4, NVP-1.8, and NVP-2.2 samples above T_g .

internal residual stress. To avoid a catastrophic loss of the strength above T_g caused by the hyperactive polymer segments, the NVP-2.2 samples that exhibit high tensile strength was selected to evaluate the mechanical behavior (Fig. 2i). It shows that above T_g the NVP-2.2 samples still retain a considerable tensile strength of 3.01 MPa and a fractural strain of 281 %, respectively. This comparison study illustrates that NVP as a hard segment imparts strength to the adhesives, making it more difficult to deform, while DA as a soft segment improves the stretchability of the adhesives. Thus, combination of these soft and hard monomers with different ratios in the ink imparts the synthesized SMP with high tunability in mechanical properties.

T_g of the materials was measured by dynamic mechanical analysis (DMA). The DMA curves shown in Fig. 3a-c indicate that as the temperature increases above T_g , the storage modulus of the materials decreases exponentially, indicating a transition from a glassy state to a rubbery state [28]. Dependence of T_g on the content of DA, HA, and NVP was derived from Fig. 3a-c and summarized in Fig. 3d. It shows that as the weight ratio of DA increases, T_g decreases from 22 to 17 °C. It can be attributed to the effect of the long, soft fatty acid chains. In contrast, as the weight ratios of HA, NVP increase, T_g increases from 22 to 29 °C and from 22 to 38 °C, respectively. That could be because the ring structures in HA and NVP as well as the formed H-bonds by HA increase the rigidity and lower the motion of the polymer chains [29]. To optimize the shape memory performance at different temperatures, the weight ratios of the monomers can be varied accordingly. For example, Fig. 3e shows a shape memory cycle of an NVP-2.2 strip. It was programmed to a temporary shape at a maximum strain of ~200 % at 70 °C. This programmed

shape was then fixed below T_g , and then recovered to its original shape when heated above T_g (Video S2). Moreover, we also studied the shape fixing and recovery ratios. In the test, the SMPs were first applied with a programmed strain (ε_p) of 100 % above T_g . Then, the temperature was gradually lowered below T_g while keeping the material isothermally at 100 % strain for 2 min. The retained strain ε_u was obtained after removing the external load. Then temperature was raised above T_g , the shape was recovered. The residue strain ε_r was measured. The shape fixing ratio $R_f = \varepsilon_u/\varepsilon_p$ and recovery ratio $R_r = (\varepsilon_u - \varepsilon_r)/\varepsilon_u$ were calculated. Their dependences on the weight ratios of the three monomers were quantified and shown in Fig. 3f-h. Thanks to the flexible linear chains, the SMPs maintain >95 % of R_r . Although R_f values vary with the change of the weight ratios of the monomers, they still show >85 %. In contrary to HA and NVP, the long fatty acids chains in DA promote chain flexibility, which reduces the R_f values as the DA ratio increases. This is consistent with the phenomenon showing a smaller residual strain in the SMPs with high DA weight ratios (Fig. 2g-h).

2.3. Adhesion performance and mechanism

This developed SMP adhesive exhibits considerable adhesion strength to different types of substrates owing to its microstructure and the R2G adhesion mechanism. In its rubbery state, the polymer chains facilitate formation of H-bonds with the substrates (Fig. 4a) [16]. For example, a DA-3.2 sample with T_g of 17 °C remains a rubbery state at room temperature. Thus, in the room temperature water (~20 °C) it exhibits adhesion to surfaces of seashell, wood, plastics (polyethylene

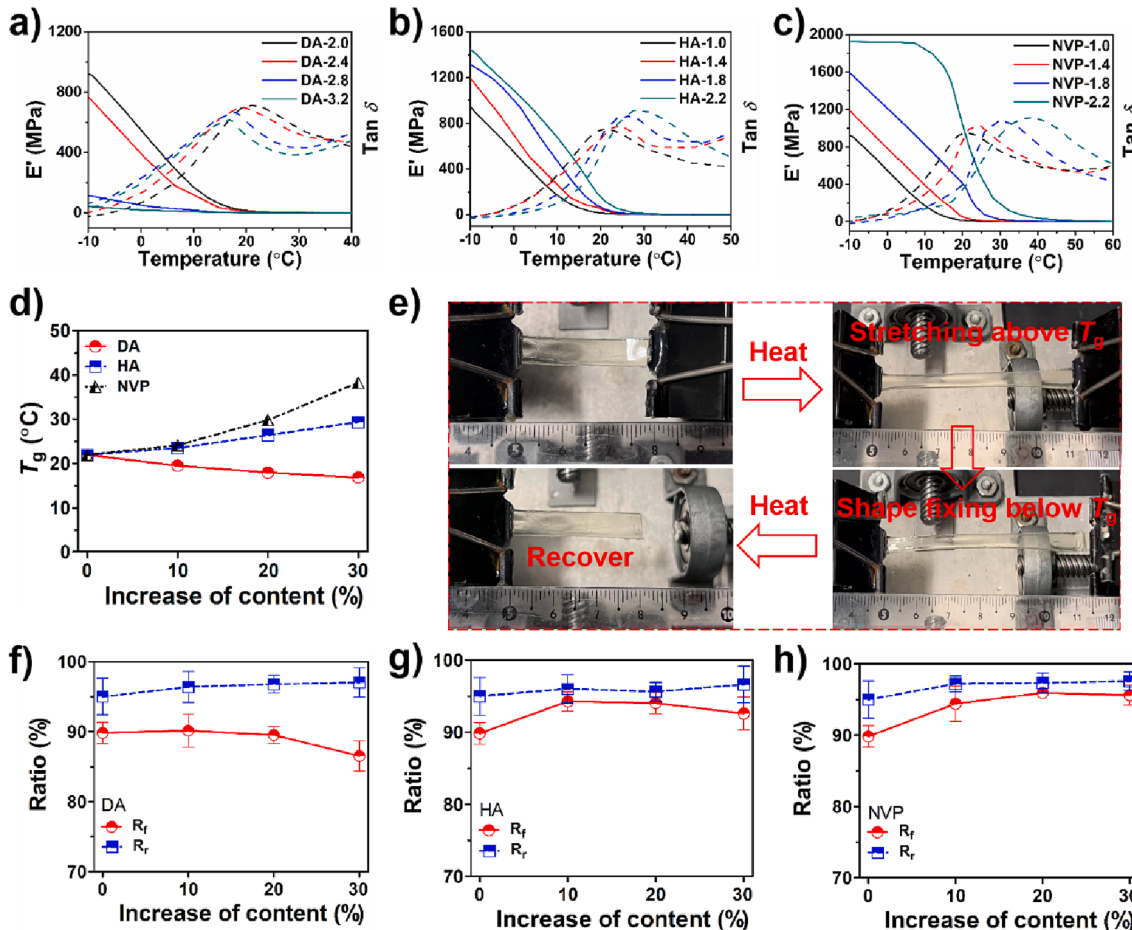


Fig. 3. Storage modulus (solid lines)-damping parameters (dash lines) of the SMP adhesives with different (a) DA, (b) HA, and (c) NVP ratios. (d) T_g of the SMPs vs. weight ratios of the three monomers in the ink. (e) Photographs showing a shape memory cycle of a SMP adhesive with a DA:HA:NVP ratio of 2:1:2.2. Shape fixing ratio R_f and shape recovery ratio R_r of the SMPs with different (f) DA, (g) HA, and (h) NVP ratios.

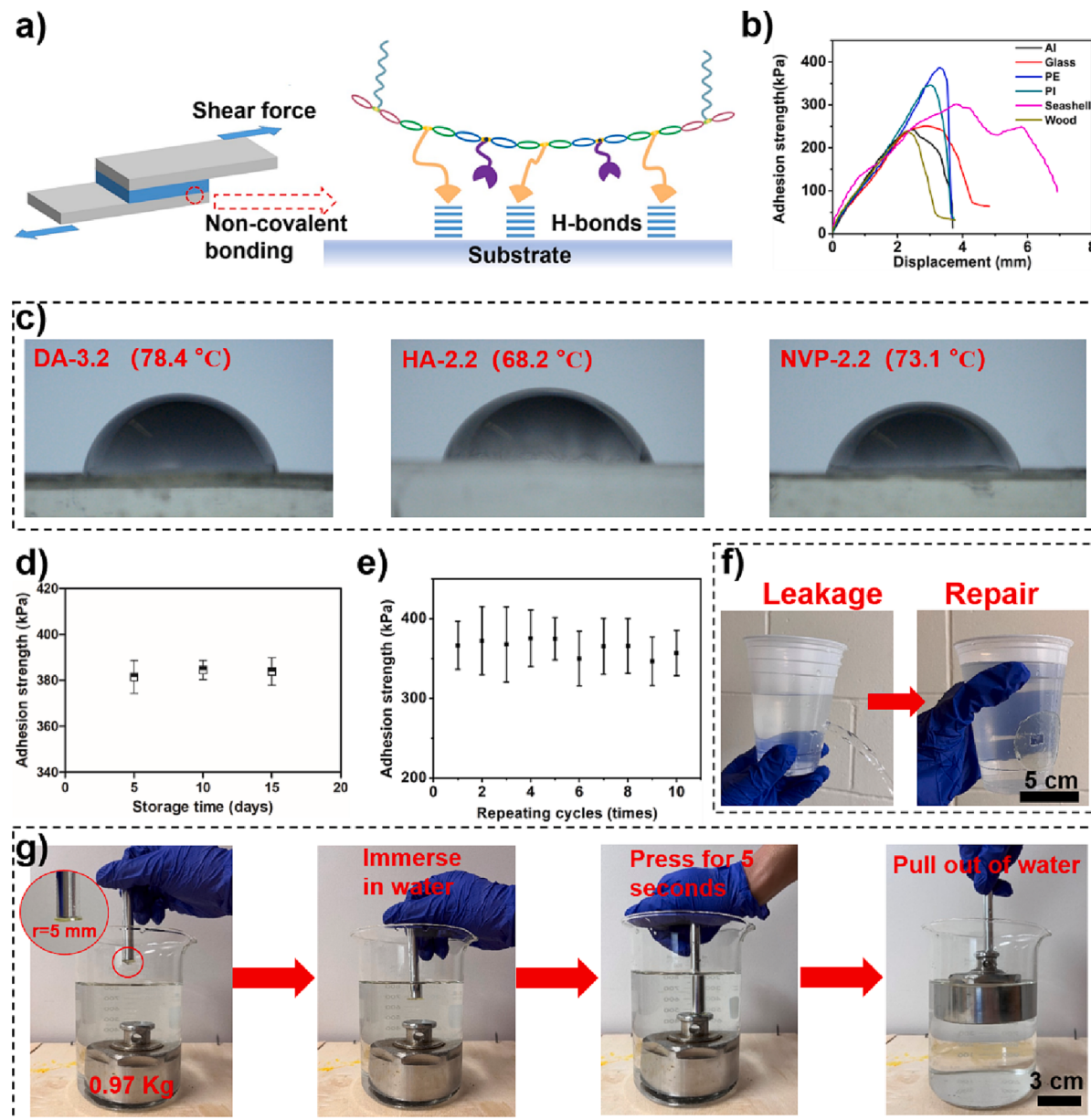


Fig. 4. (a) Schematic showing adhesion mechanism enabled by H-bonding. (b) Shear stress-strain curves of DA-3.2 adhered to various substrates. (c) Photographs showing the contact angles of the SMP adhesives. (d) Adhesion strength of DA-3.2 adhered to PE after immersed in water for different durations. (e) Cyclability test to show reversible wet adhesion of DA-3.2 to PE. (f) Photographs showing DA-3.2 adhered to a plastic cup for leakage repairing. (g) Photographs showing DA-3.2 adhered underwater to a weight which was easily lifted.

(PE), polyimide (PI)), glass, and aluminum (Al) (Fig. S3). Shear tests were then conducted to measure adhesion strength between the adhesive and these substrates. Stress-strain curves in Fig. 4b show that the adhesion strength to all the substrates is >200 kPa, with the ones adhered to PE and PI being close to 400 kPa, while porous wood exhibits relatively lower adhesive strength as the water droplets are trapped at the interfaces of the substrates and adhesives. In addition, the contact angles increase from 68.2 to 78.4 °C with the increased weight content of DA (Fig. 4c). It is important to note that the primary role of DA is to protect the adhesion by reducing the direct contact of water with the H-bonds. The increased contact angle indicates an enhanced hydrophobicity of the adhesive, which helps to prevent water penetration and maintain the adhesion strength. As shown in Fig. S4, the water uptake of the SMP adhesives is negligible after being soaked in water for 15 days. This great hydrophobicity can partially explain why the hydrophilic H-bonds can be protected from water infiltration to weaken the bonding in

the interfaces. Thus, the underwater bonding remains stable for at least 15 days (Fig. 4d).

The instant adhesion can be reversible (Fig. 4e). Although it shows a little reduction in the adhesion strength after 10 times, it can be recovered after the adhesive surface is cleaned with alcohol to remove accumulated dust. Meanwhile alcohol would break H-bonds of adhesive and consequently reduces the adhesion strength, which makes the adhesive be easily peeled off the substrates (Fig. S5 and Video S3). As shown in Fig. S6, the adhesion strength of DA-3.2 adhered to PE is reduced by $\sim 87\%$ after soaked in alcohol for 3 s. A significant reduction of 96 % and 97 % in the adhesion strength on the wood and seashell surfaces is observed. This could be because the high roughness surfaces allow the alcohol to better penetrate the interfaces, thus causing debonding. The exhibited adhesion properties make it be easily adhered to a plastic cup at room temperature in a few seconds for repairing water leak (Fig. 4f and Video S4). Additionally, after it is adhered to a weight with 0.97 kg

underwater, the adhesive with only 5 mm in radius can easily lift the weight (Fig. 4g and Video S5).

The adhesive exhibits the R2G adhesion mechanism, or called structural bonding, enabled by its shape memory property to further increase the adhesion strength. The mechanism is illustrated in Fig. 5a. In its rubbery state above T_g , the adhesive can conform to rough and uneven surfaces under an external force. Below T_g , the adhesive retains its shape with an increasing modulus (glassy state), thus forming mechanically interlocked structural bonding. By this way, the adhesion strength is increased. To verify this hypothesis, we used NVP-2.2 as a demo sample. First, above T_g , NVP-2.2 was conformably contacted with the striated surface of a seashell. The mosaic pattern of the surface was

transfer printed to the NVP-2.2 film, which was then fixed when the temperature was below T_g . This transferred pattern was recovered to the originally flat surface above T_g (Fig. 5b). To test if this shape memory property can be achieved at a micrometer scale, micro-patterns of grid, strip, and letter were programmed by transfer printing, fixed, and then recovered on the NVP-2.2 films by the same way (Fig. 5c, Fig. S7, and Video S6). This interlocked micro-pattern does have the effect of preventing the separation of the substrate from the adhesive during the shear stretching (Fig. S8).

These results motivate us to explore the effect of surface roughness on the adhesion strength. To do that, three brass samples with different surface roughness ($R_1 = 1.32 \mu\text{m}$, $R_2 = 0.42 \mu\text{m}$, $R_3 = 0.11 \mu\text{m}$) were

(a) Schematic showing the R2G adhesion mechanism. It illustrates the adhesive's behavior in three states: **below T_g** (blue bar), **above T_g** (yellow bar), and **below T_g** again (blue bar). The process involves **heat up** (transition from blue to yellow) and **cool down** (transition from yellow back to blue). A **locked** state is shown where the adhesive conforms to a rough surface under **force**.

(b) Photos showing the **Attach above T_g and fix below T_g** , **Adapt to the surface**, and **Recover to original shape above T_g** steps.

(c) Photos showing the **Pattern** and **Smooth** states, with a 500 μm scale bar.

(d) SEM image of the NVP-2.2 surface with a 10 μm scale bar.

(e) Adhesion strength (kPa) vs Displacement (mm) for three roughness levels: R_1 (black), R_2 (red), and R_3 (blue). The curves show an initial peak followed by a drop-off.

(f) Photos demonstrating an active SMP valve, showing the valve opening in cold water and closing in hot water.

(g) Adhesion strength (kPa) vs Displacement (mm) for HA-2.2 and PE adhesives above and below T_g .

(h) Adhesion strength (kPa) vs Displacement (mm) for PI adhesives above and below T_g .

(i) Log-log plot of Adhesion strength (kPa) vs Time of bonding (min) for various materials, including **Polymer coatings [30]**, **Plastic films [1, 31, 32]**, **Elastomers [33]**, **Hydrogels [8, 34-44]**, and **This work**.

(j) Three finite element simulation plots showing the de-bonding process with a color scale from **Max** (red) to **Min** (blue).

(k) Force (N) vs Displacement (mm) for three roughness levels: R_1 (black), R_2 (red), and R_3 (blue).

Fig. 5. (a) Schematic showing R2G adhesion mechanism enabled by shape memory. Shape programming, fixation, and recovery of an NVP-2.2 film transfer printed from: (b) a surface of a seashell; (c) a grid micro-pattern. (d) A SEM image of the NVP-2.2 surface programmed from the brass surface with roughness of R_1 . (e) Adhesion stress-strain curves of NVP-2.2 to three brass samples with different roughness levels. (f) Demonstration of an active SMP valve. SMP share stress-strain curves of (g) HA-2.2 and (h) NVP-2.2 adhered to PI and PE above and below T_g . (i) Comparison of adhesion strength of the different types of adhesives. Finite element simulation on (j) de-bonding process; (k) de-bonding shear force–displacement curves of the SMP adhesives adhered to surfaces with three different roughness levels.

6

prepared (Fig. S9). Fig. 5d and Fig. S10 show the SEM images of an NVP-2.2 adhesive with a programmed shape transfer printed from the brass sample with surface roughness of R1, from which a sub-micrometer feature can be observed. Fig. 5e shows the shear stress test of the adhesives to these three types of brass samples with their statistic results summarized in Fig. S11. It shows that the average adhesive strength to the brass surfaces with R1, R2, and R3 roughness is 409 kPa, 330 kPa, and 250 kPa, respectively. This suggests that increased surface roughness increases the adhesion strength. The strategy of combining the chemical and the structural adhesion can be applied as an active valve. As shown in Fig. 5f, an adhesive with a programmed cylindrical shape (Fig. S12) was inserted into an open tube in a funnel. Due to existence of a gap between the tube and the stretched shape of the adhesive, cold water flowed through the tube, while hot water ($\sim 60^\circ\text{C}$) was blocked by the SMP valve. As its shape recovered above T_g induced by the hot water, the valve expanded and adhered to the tube surface (Video S7). Fig. S13 shows that the adhesive was adhered to the surface of a glass container with hot water above T_g . When the temperature was below T_g , the adhesion strength was improved so that the container was easily lifted (Video S8).

To quantify the R2G adhesion, the adhesives were bonded to PE and PI above T_g and then the comparison shear stress testing was done above and below T_g . The results show that below T_g the adhesion strength of HA-2.2 adhered to PI and PE increases by 108 % and 88 % from 387 and 490 kPa tested above T_g , respectively (Fig. 5g), while below T_g , the adhesion strength of NVP-2.2 adhered to PI and PE increases by 249 % and 190 % from 228 and 314 kPa tested above T_g , respectively (Fig. 5h). As shown in Fig. 5i, when compared to the tape-type adhesives [1,8,30–44], the SMP adhesives demonstrated in this work achieved adhesion strength in a range of 238–924 kPa. Compared to adhesive hydrogels, which tend to have relatively low adhesion strength and can be easily damaged or ruptured under stress, the SMP adhesives show superior adhesion performance. It is worth mentioning that the adhesion of our SMPs can happen in <2 min. In summary, these properties are better than or comparable to the previously reported polymer or hydrogel adhesives.

Above T_g , SMP is soft and forms conformable contact with the surface texture with an applied pressure. Below T_g , the shape can be locked with much improved mechanical strength, which is combined with the enhanced interfacial area to afford greatly improved shear strength. To validate the mechanism, the finite element analysis (FEA) was performed to simulate how the shape transition can improve the adhesion using a single lap joint as a model (Fig. 5j and Video S9). The numerical (Fig. 5k) results show the shear strength becomes larger as the roughness (simulated by the amplitude of sinuous functions) is increased, which is consistent with experimental results (Fig. 5e). Fig. 5k also proves that the roughness imparts structure resistance to SMP to increase the shear stiffness and strength. Meanwhile, it is found that the polymerization degree also affects the adhesion strength. As shown in Fig. S14, the relationship between the molecular weight of the polymer and the tensile, adhesion strength was investigated. Adding more NVP and HA will promote the internal H-bond formation, thereby increasing the cohesion among the polymer chains. This observation is also intuitively reflected in the increased molecular weight of the polymer. Improving the shear resistance of the adhesive makes it easier to adhere to the substrate.

2.4. Underwater adhesion for on-skin sensor application

An application of an underwater adhesive is to be used for on-skin electronics. Before testing such durability, a biocompatibility test of the adhesive should be conducted. Thanks to its bio-based content, the cells can proliferate when co-cultured with the SMP adhesive surface for 4 days (Fig. S15). It should be noted that the average counts of the co-cultured cells are high with a cell viability of $>80\%$ (Fig. S16). When the average value was 50 % or higher, the percentage of cell viability

was deemed optimal in other studies for evaluating the cytotoxicity of the materials [45]. Therefore, this adhesive is not cytotoxic to cells, which is consistent with the results shown in other studies about the cytotoxicity of similar materials for on-skin applications [46,47]. After testing the biocompatibility, we evaluated and compared the signal acquisition performance of a commercial hydrogel electrode and a commercial conductive electrode encapsulated with the developed SMP adhesive for electromyography (EMG) recording. As shown in Fig. S17, after 1 min underwater test, the hydrogel electrode swelled a lot due to water absorption and was easily detached from the skin, while the one encapsulated with the SMP adhesive remained the same surface shape and was firmly adhered to the skin (Fig. S18). As a result, the EMG signals collected from the SMP electrode can be transmitted by a simple flexion motion, and the light bulb became brighter (Fig. 6a and Video S10). Due to the strong and conformable adhesion to the skin, the conductive electrode capsuled with the SMP adhesive can record the EMG signals with such a high fidelity, where the collected EMG spectra for various types of muscle motions can be distinguished. Fig. 6b-c show the EGM signals collected from the two different muscle motions. One is from flexion, a muscle motion that produces a high, sharp signal shape. The other is from twist, a small, slow muscle motion that produces a small, broad signal shape. Because of these high-fidelity EMG signals recorded underwater, we conceived a Morse coding system, a way to transmit various kinds of information through defined flexion and twist motions. They are defined as “dots” and “dashes”, respectively (Fig. 6d). With these Morse codes, various Latin alphabet can be transmitted through arm motions for a purpose of transmitting underwater immittance information. For instance, letter “S” can be represented by three continuous flexion motions and letter “O” can be interpreted by three continuous twist arm motions. Accordingly, the message “SOS” and “HELP” can be effectively transmitted via the EMG signals by swinging arms underwater (Fig. 6e and f).

3. Conclusion

This study presents a novel strategy of combining chemical interactions and structure bonding in a photocured, bio-based shape memory thermoplastics for reversible, repeatable underwater adhesion. Hydrophobic interactions empowered by the long fatty acid chains in the polymerized SMP can protect the non-covalent hydrogen interactions from being destroyed by the water molecules in the interfaces. The SMP has reasonable T_g in a range of $17\text{--}38^\circ\text{C}$, making the R2G adhesion enabled by the shape locking effect, or called structural bonding, be easily achieved. The protected hydrogen interactions and enhanced R2G adhesion by the shape memory effect make the fabricated SMP adhesive realize adhesion strength of up to 924 kPa. The adhesion is instant and reversible. It was demonstrated the applications in repairing water leaks, strong underwater adhesion for long-lasting, high-fidelity underwater EMG signal recording. This proposed strategy would pave a new, general way to designing and synthesizing high-performance bio-based underwater adhesives from renewable sources.

4. Methods

4.1. Materials

2-Hydroxy-3-phenoxypropyl acrylate (HA), *N*-Vinylpyrrolidone (NVP, >99 %), and dodecyl acrylate (DA, >90 %) were purchased from Sigma Aldrich (St. Louis, MO, U.S.). Diphenyl(2,4,6-trimethylbenzoyl) phosphine oxide (TPO, >97 %) was purchased from Fisher Scientific (Pittsburgh, PA, U.S.). These materials were used without further purification.

4.2. Ink preparation and photocuring of biopolymer

DA, HA, and NVP were mixed at weight ratios of 2:1:1 as a control

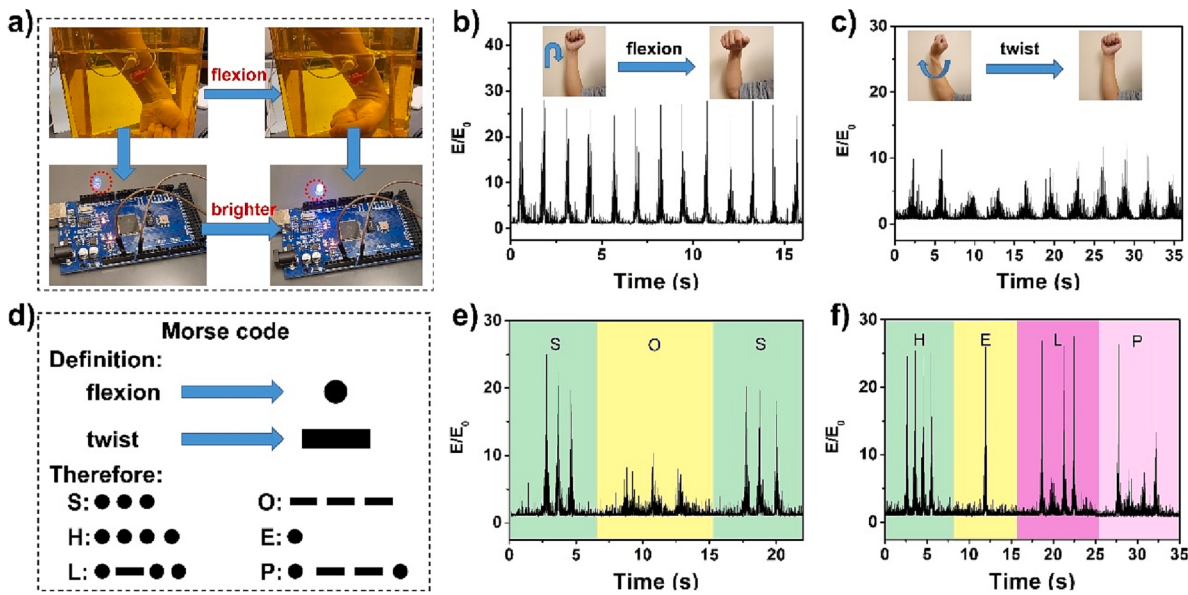


Fig. 6. (a) Flexion to control bulb brightness underwater by an EMG sensor protected by the SMP adhesive. The EMG signals caused by muscle motions of: (b) flexion and (c) twist. (d) Definition of Morse codes based on two types of the EMG signals from muscle motions of flexion and twist. Transmitted Morse codes of (e) SOS, and (f) HELP via the EMG signals by underwater muscle motions of the flexion and twist.

sample. When we studied the effect of a monomer weight ratio on the material properties, two of these monomers were fixed while the third one was increased in an incremented weight of 10 % of the ink. For example, when studying the effect of the DA weight ratio, the weight ratio of HA and NVP was kept as 1:1, and the DA weight ratio versus HA or NVP was increased from 2.0 to 2.4, 2.8, and 3.2. The obtained samples were named as DA-2.0, DA-2.4, DA-2.8, DA-3.2, respectively. The samples of HA-1.0, HA-1.4, HA-1.8, and HA-2.2 refer to the ones with the DA-HA-NVP ratios of 2:1:1, 2:1.4:1, 2:1.8:1, and 2:2.2:1, respectively. The samples of NVP-1.0, NVP-1.4, NVP-1.8, and NVP-2.2 refer to the ones with the DA-HA-NVP ratios of 2:1:1, 2:1.4, 2:1.8, and 2:1.2:2, respectively. All the resins were added with a photoinitiator, diphenyl(2,4,6-trimethylbenzoyl)phosphine oxide (TPO) (2 wt %). The ink was photocured by UV-light with an irradiation wavelength of 405 nm under a power density of $\sim 5 \text{ mW/cm}^2$. The exposure time was set to 1 min. Then, the photocured objects were post-cured in a 405-nm UV light oven for 6 min.

4.3. Materials characterization

The viscosity of ink was evaluated by a modular rotation and interface rheometer MCR302 equipped with a C60/2°. The test was performed at room temperature with shear rates changing from 0.1 to 100 1/s. The glass transition temperature (T_g) of the polymer was obtained from differential scanning calorimetry (DSC) and dynamic mechanical analysis (DMA). DSC was monitored by using a DSC Q20 machine (TA Instruments, Newcastle, DE, USA). Samples with a weight of $\sim 15 \text{ mg}$ was placed in a standard aluminum crucible with a lid and were scanned in a dynamic mode from -10 to 100°C at a heating rate of $10^\circ\text{C}/\text{min}$ under N_2 atmosphere (30 mL/min). DMA (testing sample: 50 mm length, 5 mm width) test was performed on a DMA 7100 machine (Hitachi, Chiyoda, Tokyo, Japan). Measurement was conducted from -10 to 100°C in a tensile mode. The heating rate was $3^\circ\text{C}/\text{min}$ and the frequency was 1 Hz. Fourier transform infrared (FTIR) spectra were collected by a Thermo Nicolet 380 FTIR Spectrometer with DIAMOND ATR. Gel permeation chromatography (GPC) measurements were performed by high performance liquid chromatograph (HPLC) (Agilent 1200 series, Agilent Technologies, Palo Alto, CA) equipped with a refractive index (RI) detector and an Agilent PLgel 5 μm MIXED-D column. The measurements were performed at 35°C with Tetrahydrofuran

(1 mL/min) as the eluent. Polystyrene was used as standards for calibration. SEM images were collected using a Thermoscientific Volumescope at an accelerating voltage of 5.0 kV. The samples were coated with a thin gold film (10 nm) before imaging. The optical images were obtained by Amscope FMA050. The tensile testing was conducted on a Mark-10 universal testing machine at a moving rate of 50 mm/min. Cyclic tensile tests were conducted at a strain of $\sim 80\%$ of elongation at break at a crosshead speed of 50 mm/min. There was no waiting time between consecutive cycles (1st to 5th cycle). After five cycles, the samples were allowed to relax with a heat gun at the 6th cycle.

4.4. Roughness test

Roughness Tester AMT211 was used to extract R_a , which is the average roughness of the surface. It offers a broad assessment of surface texture height. Specifically, R_a calculates the average deviation in height for every point on the surface from the mean height. R_a is defined in the annexes of JIS B 0031 and JIS B 0601 as follows:

$$R_a = \frac{1}{l} \int_0^l |y| dx$$

The mean line is laid on a Cartesian coordinate system where the tester tip passes through x-axis and magnification is in y-axis. As R_a takes the average roughness through the entire surface, it compensates any local rough area that is not common throughout the surface.

4.5. Adhesion test

The adhesive was sandwiched between two pieces of selected substrates with 80 N preload in water or stored in water for different durations. Then, the adhered plates were clamped into a Mark-10 universal testing machine and pulled at a crosshead speed of 50 mm/min. The adhesion strength was calculated by dividing the measured maximum load by the bonded area. Four measurements were made for each type of the SMP samples. To test water absorption in the SMP samples were first dried in an oven at 50°C for 3 h, then sealed in a plastic bag. After it was cooled to room temperature, they were weighed to obtain the dry weight of the sample (m_0). The samples that were soaked in distilled water for various duration were then dried with a tissue paper, finally weighed to get average actual sample weight (m). The difference of m and m_0 is the

absorbed water weight for each sample.

4.6. Biocompatibility test

Co-culturing with pluripotent mesenchymal progenitor C3H10T1/2 cells was used to test the cytocompatibility of the SMPs. Dulbecco's Modified Eagle Medium (DMEM) supplemented with 10 % fetal bovine serum was used to grow the cells. To see how the SMPs affected C3H10T1/2 cell growth, 5x104 cells were seeded in a 6-well plate containing sterile SMP circular discs. Before loading the SMP discs into the culture medium, they were post cured for 30 min, then soaked in PBS for 48 h to remove any unreacted monomers, followed by sterilization in ethanol. Images of cells in each group were captured using a Nikon microscope after each day of culturing continuously for 4 days. Cells were dissociated with trypsin and counted using a Bio-Rad TC10 Automated Cell Counter.

4.7. FEA simulation of the R2G adhesion mechanism

We used COMSOL Multiphysics to simulate the SMP when adhered to surfaces with three different roughness levels. To reduce the computational cost, 3D elasticity problem was reduced to a 2D plane strain elasticity problem with thickness of 1 cm. The 2D geometry of a single lap joint used as a model for simulation is shown in Fig. S19. The roughness was simulated by a sinusoidal function [48] with an amplitude of A and a wavelength of 0.6 cm. The material of the laps is a steel with Young's modulus being 210 GPa, Poisson's ratio 0.3, and mass density 7800 kg/m³. The SMP adhered to the two laps was simulated as a Mooney-Rivlin model with $C_{10} = 1.5$ MPa, $C_{01} = 0.4$ MPa, and a bulk modulus $\kappa = 100$ MPa. The left side was fixed while the right side was applied by a horizontal displacement. The interfaces between SMP and laps were modeled as the contact pairs, where adhesion was formulated by the penalty method with the penalty factor (adhesive stiffness) of 20 GN/m³. For the decohesion process, we used displacement-based damage model to simulate the split of the SMP and laps. In the simulation, we selected tensile strength $\sigma_t = 2$ MPa, shear strength $\sigma_s = 3$ MPa, tensile energy release rate $G_{ct} = 1130$ J/m², shear energy release rate $G_{cs} = 1800$ J/m². The power law (exponent equals to 1) used the fracture mode criterion to study the crack evolution. To solve the nonlinear equations, we used the double dogleg method with a maximum number of 250 iterations.

Declaration of Competing Interest

The authors declare that they have no known competing financial interests or personal relationships that could have appeared to influence the work reported in this paper.

Data availability

Data will be made available on request.

Acknowledgement

J. L. thanks for the financial support awarded by the National Institutes of Health (award number: 1R03EB028922-01). G.H. acknowledges the funding support from NSF CMMI under Award No. 1930873.

Appendix A. Supplementary data

Supplementary data to this article can be found online at <https://doi.org/10.1016/j.cej.2023.144226>.

References

- [1] H. Yuk, C.E. Varela, C.S. Nabzdyk, X. Mao, R.F. Padera, E.T. Roche, X. Zhao, Dry double-sided tape for adhesion of wet tissues and devices, *Nature* 575 (7781) (2019) 169–174.
- [2] R. Hensel, K. Moh, E. Arzt, Engineering micropatterned dry adhesives: from contact theory to handling applications, *Adv. Funct. Mater.* 28 (2018) 1800865.
- [3] H. Fan, J. Wang, J.P. Gong, Barnacle cement proteins-inspired tough hydrogels with robust, long-lasting, and repeatable underwater adhesion, *Adv. Funct. Mater.* 31 (2021) 2009334.
- [4] H. Fan, J.P. Gong, Bioinspired underwater adhesives, *Adv. Mater.* 33 (2021) 2102983.
- [5] X. Li, Y. Deng, J. Lai, G. Zhao, S. Dong, Tough, long-term, water-resistant, and underwater adhesion of low-molecular-weight supramolecular adhesives, *J. Am. Chem. Soc.* 142 (11) (2020) 5371–5379.
- [6] A. Cholewiński, F.K. Yang, B. Zhao, Algae-Mussel-inspired hydrogel composite glue for underwater bonding, *Mater. Horiz.* 6 (2) (2019) 285–293.
- [7] Y. Zhao, Y. Wu, L. Wang, M. Zhang, X. Chen, M. Liu, J. Fan, J. Liu, F. Zhou, Z. Wang, Bio-inspired reversible underwater adhesive, *Nat. Commun.* 8 (2017) 1–8.
- [8] X. Liu, Q. Zhang, L. Duan, G. Gao, Bioinspired nucleobase-driven nonswellable adhesive and tough gel with excellent underwater adhesion, *ACS Appl. Mater. Interfaces* 11 (6) (2019) 6644–6651.
- [9] C. Heinzmann, C. Weder, L.M. de Espinosa, Supramolecular polymer adhesives: advanced materials inspired by nature, *Chem. Soc. Rev.* 45 (2016) 342–358.
- [10] H. Shao, R.J. Stewart, Biomimetic underwater adhesives with environmentally triggered setting mechanisms, *Adv. Mater.* 22 (6) (2010) 729–733.
- [11] H. Lee, B.P. Lee, P.B. Messersmith, A reversible wet/dry adhesive inspired by mussels and geckos, *Nature* 448 (7151) (2007) 338–341.
- [12] Z. Ma, G. Bao, J. Li, Multifaceted design and emerging applications of tissue adhesives, *Adv. Mater.* 33 (2021) 2007663.
- [13] S. Ji, C. Wan, T. Wang, Q. Li, G. Chen, J. Wang, Z. Liu, H. Yang, X. Liu, X. Chen, Water-resistant conformal hybrid electrodes for aquatic endurable electrocardiographic monitoring, *Adv. Mater.* 32 (2020) 2001496.
- [14] X. Wan, Z. Gu, F. Zhang, D. Hao, X. Liu, B. Dai, Y. Song, S. Wang, Asymmetric Janus adhesive tape prepared by interfacial hydrosilylation for wet/dry amphibious adhesion, *NPG Asia Mater.* 11 (2019) 1–9.
- [15] J.K. Park, J.D. Eisenhaure, S. Kim, Reversible underwater dry adhesion of a shape memory polymer, *Adv. Mater. Interfaces* 6 (2019) 1801542.
- [16] Y. Wu, Y. Chen, Y. Zeng, C. Li, R. Qiu, W. Liu, Photo-curing preparation of biobased underwater adhesives with hydrophobic chain-ring interface structure for protecting adhesion, *Appl. Mater. Today* 27 (2022), 101436, <https://doi.org/10.1016/j.apmt.2022.101436>.
- [17] H. Zheng, J. Li, Y. Zhou, C. Zhang, W. Xu, Y. Deng, J. Li, S. Feng, Z. Yi, X. Zhou, Electrically switched underwater capillary adhesion, *Nat. Commun.* 13 (2022) 4584.
- [18] S. Baik, D.W. Kim, Y. Park, T.-J. Lee, S. Ho Bhang, C. Pang, A wet-tolerant adhesive patch inspired by protuberances in suction cups of octopuses, *Nature* 546 (7658) (2017) 396–400.
- [19] J. Shi, Y. Ye, N. Luo, L. Zhang, J. Wang, T. Lin, J. Yang, L. Ye, Y. Li, J. You, Substrate-independent, robust and functional Pvdf-G-II coating based on tunable surface free energy, *Appl. Surf. Sci.* 618 (2023), 156613.
- [20] Y. Xia, Y. He, F. Zhang, Y. Liu, J. Leng, A review of shape memory polymers and composites: mechanisms, materials, and applications, *Adv. Mater.* 33 (2021) 2000713.
- [21] C. Linghu, X. Yang, Y. Liu, D. Li, H. Gao, K.J. Hsia, Mechanics of shape-locking-governed R2g adhesion with shape memory polymers, *J. Mech. Phys. Solids* 170 (2023), 105091, <https://doi.org/10.1016/j.jmps.2022.105091>.
- [22] Y. Wu, Y. Zeng, Y. Chen, C. Li, R. Qiu, W. Liu, Photocurable 3d printing of high toughness and self-healing hydrogels for customized wearable flexible sensors, *Adv. Funct. Mater.* 31 (2021) 2107202, <https://doi.org/10.1002/adfm.202107202>.
- [23] Y. Wu, M. Fei, T. Chen, C. Li, T. Fu, R. Qiu, W. Liu, H-bonds and metal-ligand coordination-enabled manufacture of palm oil-based thermoplastic elastomers by photocuring 3d printing, *Addit. Manuf.* 47 (2021), 102268, <https://doi.org/10.1016/j.addma.2021.102268>.
- [24] B. Zhang, H. Li, J. Cheng, H. Ye, A.H. Sakhaei, C. Yuan, P. Rao, Y.-F. Zhang, Z. Chen, R. Wang, X. He, J. Liu, R. Xiao, S. Qu, Q. Ge, Mechanically robust and UV-curable shape-memory polymers for digital light processing based 4d printing, *Adv. Mater.* 33 (2021) 2101298, <https://doi.org/10.1002/adma.202101298>.
- [25] Y. Wu, M. Fei, T. Chen, C. Li, S. Wu, R. Qiu, W. Liu, Photocuring three-dimensional printing of thermoplastic polymers enabled by hydrogen bonds, *ACS Appl. Mater. Interfaces* 13 (2021) 22946–22954, <https://doi.org/10.1021/acsami.1c02513>.
- [26] Y. Ma, Y. Liu, H. Su, L. Wang, J. Zhang, Relationship between hydrogen bond and viscosity for a series of pyridinium ionic liquids: molecular dynamics and quantum chemistry, *J. Mol. Liq.* 255 (2018) 176–184, <https://doi.org/10.1016/j.molliq.2018.01.121>.
- [27] M. Fujimura, T. Hashimoto, H. Kawai, Structural change accompanied by plastic-to-rubber transition of Sbs block copolymers, *Rubber Chem. Technol.* 51 (1978) 215–224.
- [28] Y. Wu, M. Fei, T. Chen, R. Qiu, W. Liu, Biocomposites from bamboo fibers and palm oil-based thermosets: effects of natural phenolic cross-linkers, *Compos. Commun.* 22 (2020), 100489, <https://doi.org/10.1016/j.coco.2020.100489>.
- [29] K. Chen, Y. Zhou, S. Han, Y. Liu, M. Chen, Main-chain fluoropolymers with alternating sequence control via light-driven reversible-deactivation

- copolymerization in batch and flow, *Angew. Chem. Int. Ed.* 61 (2022) e202116135.
- [30] Y. Ahn, Y. Jang, N. Selvapalam, G. Yun, K. Kim, Supramolecular velcro for reversible underwater adhesion, *Angew. Chem. Int. Ed.* 52 (11) (2013) 3140–3144.
- [31] C. Liu, X. Liu, C. Liu, N. Wang, H. Chen, W. Yao, G. Sun, Q. Song, W. Qiao, A highly efficient, situ wet-adhesive dextran derivative sponge for rapid hemostasis, *Biomaterials* 205 (2019) 23–37.
- [32] A. Martinelli, G.A. Carru, L. D'Ilario, F. Caprioli, M. Chiaretti, F. Crisante, I. Francolini, A. Piozzi, Wet adhesion of buckypaper produced from oxidized multiwalled carbon nanotubes on soft animal tissue, *ACS Appl. Mater. Interfaces* 5 (10) (2013) 4340–4349.
- [33] J. Liu, S. Wang, Q. Shen, L. Kong, G. Huang, J. Wu, Tough underwater super-tape composed of semi-interpenetrating polymer networks with a water-repelling liquid surface, *ACS Appl. Mater. Interfaces* 13 (1) (2021) 1535–1544.
- [34] G. Ju, M. Cheng, F. Guo, Q. Zhang, F. Shi, Elasticity-dependent fast underwater adhesion demonstrated by macroscopic supramolecular assembly, *Angew. Chem. Int. Ed.* 57 (29) (2018) 8963–8967.
- [35] X. Su, Y. Luo, Z. Tian, Z. Yuan, Y. Han, R. Dong, L. Xu, Y. Feng, X. Liu, J. Huang, Ctenophore-inspired hydrogels for efficient and repeatable underwater specific adhesion to biotic surfaces, *Mater. Horiz.* 7 (10) (2020) 2651–2661.
- [36] X. Liu, Q. Zhang, L. Duan, G. Gao, Tough adhesion of nucleobase-tackified gels in diverse solvents, *Adv. Funct. Mater.* 29 (2019) 1900450.
- [37] X. Liu, Q. Zhang, G. Gao, DNA-inspired anti-freezing wet-adhesion and tough hydrogel for sweaty skin sensor, *Chem. Eng. J.* 394 (2020), 124898.
- [38] X. Wei, D. Chen, X. Zhao, J. Luo, H. Wang, P. Jia, Underwater adhesive Hpmc/Siwpdmaema/Fe³⁺ hydrogel with self-healing, conductive, and reversible adhesive properties, *ACS Appl. Polym. Mater.* 3 (2) (2021) 837–846.
- [39] S. Bai, X. Zhang, P. Cai, X. Huang, Y. Huang, R. Liu, M. Zhang, J. Song, X. Chen, H. Yang, A silk-based sealant with tough adhesion for instant hemostasis of bleeding tissues, *Nanoscale Horiz.* 4 (6) (2019) 1333–1341.
- [40] J.N. Lee, S.Y. Lee, W.H. Park, Bioinspired self-healable polyallylamine-based hydrogels for wet adhesion: synergistic contributions of catechol-amino functionalities and nanosilicate, *ACS Appl. Mater. Interfaces* 13 (15) (2021) 18324–18337.
- [41] Z. Zhang, L. Guo, J. Hao, Emulsion-based organohydrogels with switchable wettability and underwater adhesion toward durable and ecofriendly marine antifouling coatings, *ACS Appl. Polym. Mater.* 3 (6) (2021) 3060–3070.
- [42] Z. Yu, P. Wu, Underwater communication and optical camouflage ionogels, *Adv. Mater.* 33 (2021) 2008479.
- [43] Z. Yu, P. Wu, A highly transparent ionogel with strength enhancement ability for robust bonding in an aquatic environment, *Mater. Horiz.* 8 (7) (2021) 2057–2064.
- [44] L.C. Bradley, N.D. Bade, L.M. Mariani, K.T. Turner, D. Lee, K.J. Stebe, Rough adhesive hydrogels (rad gels) for underwater adhesion, *ACS Appl. Mater. Interfaces* 9 (33) (2017) 27409–27413.
- [45] C.V. Bin, M.C. Valera, S.E.A. Camargo, S.B. Rabelo, G.O. Silva, I. Balducci, C.H. R. Camargo, Cytotoxicity and genotoxicity of root canal sealers based on mineral trioxide aggregate, *J. Endodont.* 38 (4) (2012) 495–500.
- [46] A. Tsatsakis, A.K. Stratidakis, A.V. Goryachaya, M.N. Tzatzarakis, P.D. Stivaktakis, A.O. Docea, A. Berdiaki, D. Nikitovic, K. Velonia, M.I. Shtilman, A.K. Rizos, A. N. Kuskov, In vitro blood compatibility and in vitro cytotoxicity of amphiphilic Poly-N-Vinylpyrrolidone nanoparticles, *Food Chem. Toxicol.* 127 (2019) 42–52.
- [47] N. Pippa, D. Stellas, A. Skandalis, S. Pispas, C. Demetzos, M. Libera, A. Marcinkowski, B. Trzebicka, Chimeric lipid/block copolymer nanovesicles: physico-chemical and bio-compatibility evaluation, *Eur. J. Pharm. Biopharm.* 107 (2016) 295–309.
- [48] M.L. Raffa, F. Lebon, G. Vairo, Normal and tangential stiffnesses of rough surfaces in contact via an imperfect interface model, *Int. J. Solids Struct.* 87 (2016) 245–253.